Available online at www.sciencedirect.com
ScienceDirect
ELSEVIER
PHOTONICS AND NANOSTRUCTURES Fundamentals and Applications
Photonics and Nanostructures – Fundamentals and Applications xxx (2015) xxx–xxx
www.elsevier.com/locate/photonics

Photonic crystal nanoslotted parallel quadrabeam integrated cavity for refractive index sensing with high figure of merit

Q1 Daquan Yang, Huiping Tian*, Yuefeng Ji

State Key Laboratory of Information Photonics and Optical Communications, School of Information and Communication Engineering, Beijing University of Posts and Telecommunications, Beijing 100876, China

Received 24 October 2014; accepted 26 January 2015

Abstract

Sensitivities (S) and quality factors (Q) have been trade-offs in optical resonator sensors, and optimal geometry that maximizes both factors is under active development. In this paper, we experimentally demonstrate an optical sensor based on photonic crystal (PhC) nanoslotted parallel quadrabeam integrated cavity (NPQIC) with high figure of merit (FOM). Both high sensitivity (S) of 451 nm/RIU (refractive index unit) and Q-factor >7000 in water at telecom wavelength range have been achieved simultaneously, which features a sensor figure of merit (FOM) >2000, an order of magnitude improvement over previous photonic crystal sensors.

Q3 *Keywords:* Sensitivity; Q-factor; Optical sensors; Photonic crystal; Nanoslot; Integrated cavity; FOM

1. Introduction

Q4 Over the past decades, optical micro-resonators have been widely used in optical sensors, which have attracted considerable interest for lab-on-chip applications [1]. In recent years, significant research has focused on achieving higher sensitivities (S) or higher quality factors (Q) in chip-integrated label-free biosensors [2,3]. So far, many micro-photonic devices or platforms based on photonic crystals (PhCs) [4–18], surface plasmon resonators (SPR)[19–21], interferometers [22–24], and ring resonators [25,26] have been proposed to realize optical sensors. For these sensors mentioned above, the figure of merit can be defined as $FOM = S \cdot Q/\lambda_{res}$ [27], where $S = \Delta\lambda/\Delta n$ is the refractive index sensitivity, which characterizes the shift of resonant wavelength ($\Delta\lambda$) in response to the surrounding index change (Δn), Q is the quality factor of the resonant cavity, and λ_{res} is the cavity resonant wavelength.

However, sensitivities (S) and quality factors (Q) have been trade-offs in optical resonant sensors [14], which limits the FOM: to achieve high S, the optical mode needs to overlap strongly with the detecting target (i.e. outside of the wave guiding medium), yet in order to achieve a higher Q, the optical mode should be more localized in the wave guiding medium. For example, Lai et al. [12] demonstrated photonic crystal sensors with high Q-factors ∼7000. However, S was limited to ∼60 nm/RIU (refractive index unit), and resulting in FOM limited ∼300. Wang et al. [18] demonstrated

* Corresponding author.
E-mail address: hptian@bupt.edu.cn (H. Tian).

http://dx.doi.org/10.1016/j.photonics.2015.01.008

Please cite this article in press as: D. Yang, et al. Photonic crystal nanoslotted parallel quadrabeam integrated cavity for refractive index sensing with high figure of merit, Photon Nanostruct: Fundam Appl (2015), http://dx.doi.org/10.1016/j.photonics.2015.01.008

large S of 900 nm/RIU in a slot double-beam waveguides/cavities. However, Q was limited to 700, resulting in FOM limited ~400.

In the previous work [14], we proposed and designed a photonic crystal nanoslotted parallel quadrabeam integrated cavity (NPQIC), that can remedy the fundamental trade-off between high sensitivity and high Q-factor in optical resonant sensors. In this paper, we experimentally demonstrate an optical sensor based on photonic crystal (PhC) nanoslotted parallel quadrabeam integrated cavity (NPQIC) with high figure of merit (FOM). Both high sensitivity (S) of 451 nm/RIU (refractive index unit) and Q-factor >7000 in water at telecom wavelength range have been achieved, which features a sensor figure of merit (FOM) >2000, an order of magnitude improvement over previous photonic crystal sensors.

2. Device fabrication

We fabricated and characterized the PhC nanoslotted parallel quadrabeam integrated cavity (PhC-NPQIC) sensor. The PhC-NPQIC sensor devices used in this experiment were fabricated from silicon-on-insulator (SOI) with 220 nm device layer on a 2 μm thick buried oxide layer. Firstly, first electron beam (E-beam) lithography (Elionix ELS-7000) was performed using XR-1541 (6% HSQ) E-beam resist spun at 4000 rpm (~100 nm thick), followed by development in MF-319. Fig. 1(a) shows the scanning electron microscope (SEM) images of PhC-NPQIC sensor device after first E-beam lithography. As seen, the demonstrated NPQIC sensor consists of a PhC nanoslotted parallel quadrabeam integrated cavity with nano-gap separations and two high-efficient in/out couplers on both sides of the NPQIC cavity. Secondly, refractive ion etching (RIE) of the exposed silicon region was performed with C_4F_8, SF_6, and Ar gases. After RIE, the silicon region under the E-beam resist will be retained, while the silicon exposed in the air will be etched and removed. Fig. 1(b) and (c) displays the SEM images of PhC-NPQIC cavity and taper coupler after refractive ion etching (RIE), respectively. As designed in [14], air hole gratings are in rectangular shape (Fig. 1(a) inset), the silicon thickness of the NPQIC sensor is 220 nm, the periodicity (lattice constant) $a = 500$ nm, the single nanobeam width $b = 200$ nm, the slotted gap between adjacent nanobeams is $w = 100$ nm, and the total width of the experimental PhC-NPQIC sensor device is 1.1 μm. The widths of the rectangular gratings are kept the same at 140 nm. The lengths of the gratings are quadratically tapered from cavity center $w_{cen} = 300$ nm to both sides $w_{side} = 225$ nm, i.e. $w_x(i) = w_x(1) + (i\text{-}1)^2(w_x(i_{max}) - w_x(1))/(i_{max} - 1)^2$ (i increases from 1 to i_{max}). The final cavity structure is symmetric to its center, and on each side, there are 40 gratings ($i_{max} = 40$) in the Gaussian mirror region and an additional 20 segments on both ends. Fig. 1(d) shows the field profile obtained from 3D finite-difference-time-domain (3D-FDTD). It is clearly seen that optical field is strongly localized in the slotted region. The interactions between optical mode and analytes will be efficiently enhanced and high refractive index sensitivity can be achieved.

Then, in order to achieve highly efficient coupling between the input/output fiber lens and the NPQIC sensor, a second E-beam lithography was performed with SU8-2002 E-beam resist to fabricate the input/output bus waveguides [28]. The microscope images of the SU8 polymer input/output bus waveguides as shown in Fig. 2.

Finally, to remove the XR-1542 E-beam resist on the sensor, an opening was defined by photolithography with S1818 photoresist. 7:1 buffered oxide etchant (BOE) was applied for 1 min, followed by rinsing in deionized (DI) water. Finally, photoresist was removed with acetone and IPA.

3. Experimental setup and optical characterization

A schematic of the measurement setup is shown in Fig. 3(a). TE-polarized light lunched from a tunable laser (Santec TSL-510) was coupled to the edge of the chip via an optical fiber (OZ optics) through a polarizer controller. The SU8 polymer waveguide couplers fabricated on-chip were designed to match the mode of the tapered fiber. Thus, light can be effectively coupled from the optical input fiber in-to NPQIC sensor device, and out-to the output fiber and finally to the detector. Fig. 3(b) shows the experimental alignment platform used for NPQIC sensor device measurements. Fig. 3(c) are the zoom-in images the experimental sensor device. As seen in Fig. 3(c), NPQIC sensor chip with connected tubes was clamped by home-made clamp and aligned to optical fibers. A microfluidic channel was fabricated with Polydimethylsiloxane (PDMS) by replica molding of a SU8 template, with dimensions 2 mm × 100 μm × 50μm (length, width and height). And two sub-millimeter diameter holes on both sides of microfluidic channel were punched into PDMS as inlet and outlet for sample delivery.

Fig. 4 shows the measured experimental transmission spectrum (top) and 3D finite-difference time-domain simulation (3D-FDTD) (bottom) of the NPQIC sensor device immersed in DI water, respectively. The NPQIC cavity has a resonant wavelength at 1536.30 nm, with

Please cite this article in press as: D. Yang, et al. Photonic crystal nanoslotted parallel quadrabeam integrated cavity for refractive index sensing with high figure of merit, Photon Nanostruct: Fundam Appl (2015), http://dx.doi.org/10.1016/j.photonics.2015.01.008

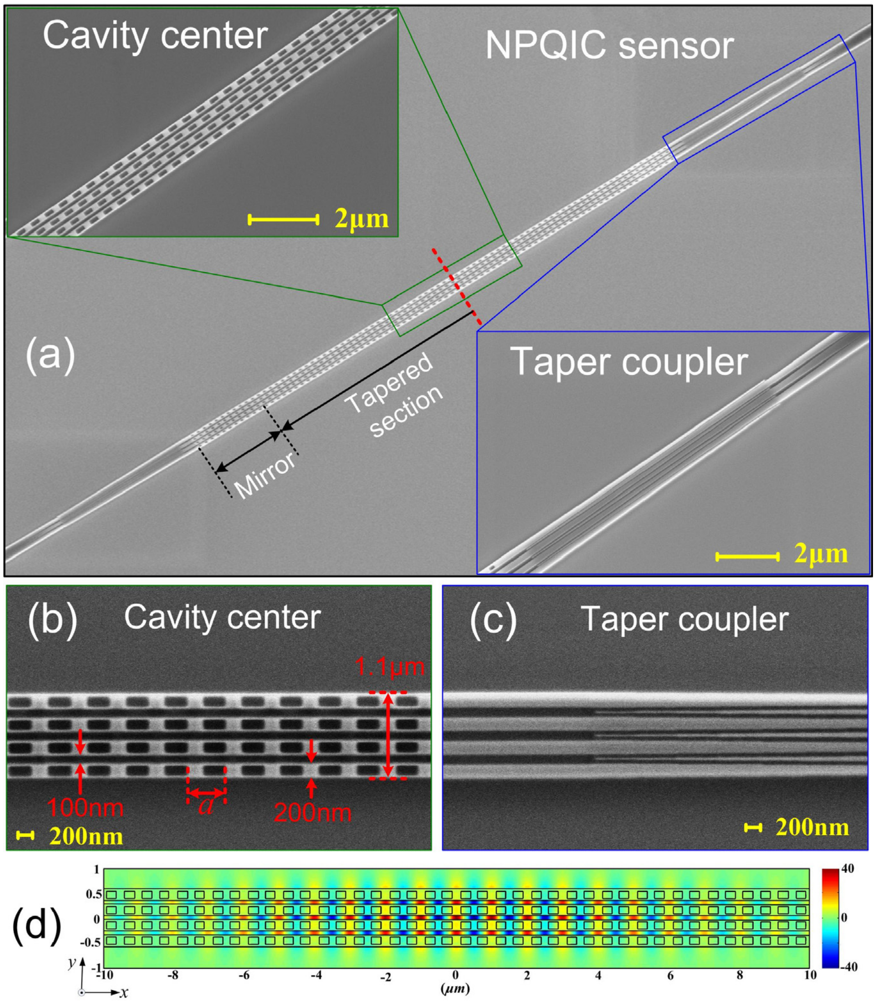

Fig. 1. (a) SEM images of the proposed Si PhC-NPQIC sensor after the first E-beam lithography, which consists of a PhC nanoslotted parallel quadrabeam integrated cavity with nano-gap separations and two high-efficient in/out couplers on both sides of the NPQIC cavity. The structure is symmetric with respect to its center (red dashed line). Inset: zoom in of the NPQIC cavity center and taper couplers, respectively. SEM images of (b) PhC-NPQIC cavity and (c) taper coupler after refractive ion etching, respectively. Here, the designed parameters: periodicity $a = 500$ nm, the single nanobeam width $b = 200$ nm, the slotted gap width w between adjacent nanobeams = 100 nm, and the total width of the experimental PhC-NPQIC
Q5 sensor device is 1.1 μm. (d) 3D FDTD simulation of the major field distribution profile (Ey) in the PhC-NPQIC. (For interpretation of the references to color in this figure legend, the reader is referred to the web version of the article.)

high Q factor of 7015, obtained from Lorenztian fitting. As seen, the experimental obtained Q value is lower than its theoretical prediction ($Q \sim 10^6$) at 1535.88 nm, primarily because of the water absorption at telecom wavelength range, surface roughness and parameter discrepancy between the designed structure and final structure after E-beam lithography and reactive ion etching processes. In addition, Q-factor of the optical cavity will be limited to the order of 10^4 due to the water absorption [29].

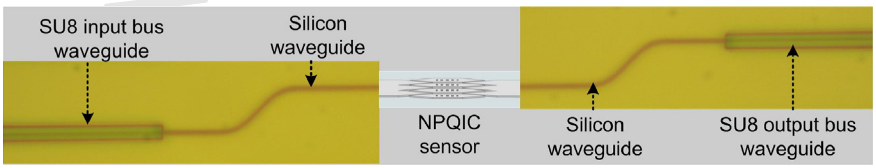

Fig. 2. The schematic of microscope image of the SU8 polymer input/output bus waveguides.

Please cite this article in press as: D. Yang, et al. Photonic crystal nanoslotted parallel quadrabeam integrated cavity for refractive index sensing with high figure of merit, Photon Nanostruct: Fundam Appl (2015), http://dx.doi.org/10.1016/j.photonics.2015.01.008

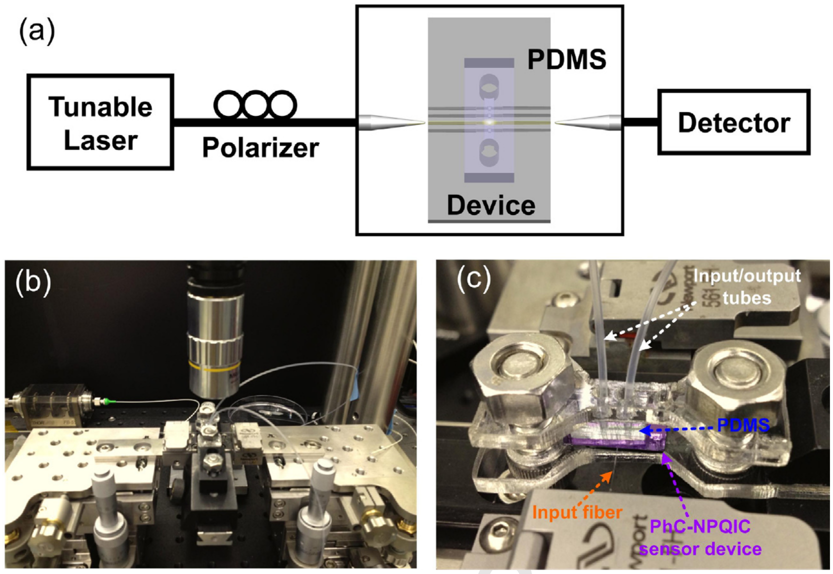

Fig. 3. (a) Schematic of the measurement setup. (b) Experimental alignment platform used for NPQIC sensor device measurements. (c) Zoom in image of the experimental sensor device with connected input/output tubes clamped by home-made clamp and aligned to optical input/output coupling fibers.

Then, in order to verify the figure of merit (FOM) of the proposed PhC-NPQIC sensor device in this paper, NPQIC sensor was calibrated with liquids of known refraction indices to characterize its response to bulk refractive index variations. Different concentrations of ethanol/water solution (volume ratio, v/v) were injected into the PDMS microfluidic channel through the tubes by syringe (Fig. 3(c)). Fig. 5 shows the resonant wavelength shifts as a function of the refractive indices controlled by different concentrations of ethanol and water. Here, the different volume ratios concentration used in our measurement are 0% (DI-water), 10%, 20%, 30%, 40%, 50%, 60%, 80%, respectively. As seen from Fig. 5, the dependence of the resonant wavelength shifts on the refractive indices is linear. The experimental bulk refractive index sensitivity $S = \Delta\lambda/\Delta n = 451$ nm/RIU is achieved, which is close to the 3D-FDTD simulation result (540 nm/RIU). Therefore, experimental FOM ($=S \cdot Q/\lambda_{res}$) of 2060 is obtained, an order of magnitude improvement over previous photonic crystal sensors

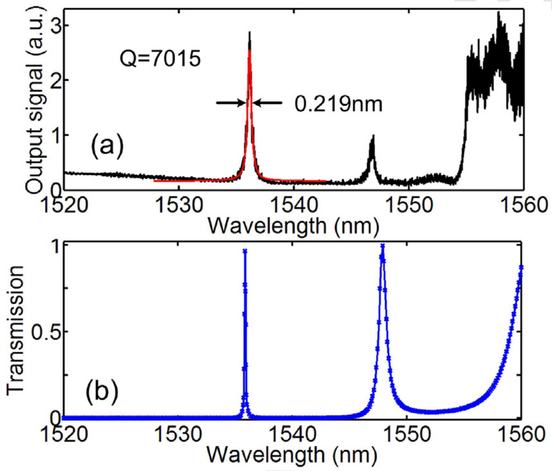

Fig. 4. (a) Experimental measured output signal (top) and (b) 3D-FDTD simulated transmission spectrum (bottom) of the silicon NPQIC sensor with the infiltration of distilled water, respectively. The resonance peak of fundamental mode at 1536.30 nm with a Lorentzian fit indicating an experimentally measured Q-factor 7015 in DI-water.

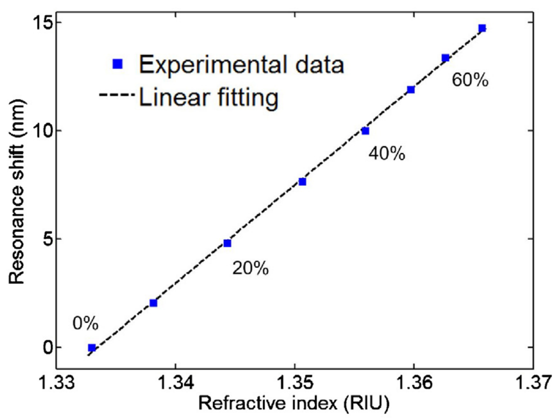

Fig. 5. Experimental resonant wavelength shifts as a function of the variations in refractive indices of different volume ratio concentrations ethanol/water solutions (v/v), changing from 0% (DI-water), 10%, 20%, 30%, 40%, 50%, 60%, 80%, respectively.

[12,18]. In addition, it is worth mentioning that the sensitivity can be even increased by suspending the cavity off the substrate.

4. Conclusion

In summary, we have experimentally demonstrated an optical sensor based on photonic crystal (PhC) nanoslotted parallel quadrabeam integrated cavity (NPQIC) with high figure of merit (FOM). A Q-factor as high as 7015 in DI-water was measured. The confined mode has a large percent of optical field energy being strongly localized in the slotted region (void space). So, the interaction between optical mode and analytes is efficiently enhanced. The parameters for the NPQIC sensor are optimized to achieve a high sensitivity while keeping a high Q-factor. We fabricated the NPQIC sensor device by E-beam lithography and characterized in ethanol/water solutions of different volume ratio concentration to confirm the numerical results. The measurement result shows a refractive index sensitivity as high as 451 nm/RIU. The figure of merit (FOM) of the NPQIC sensor over 2000 can be achieved, an order of magnitude improvement over previous photonic crystal sensors. Furthermore, considering the benefits of high Q-factor, high sensitivity, large FOM, and small footprint, we believe that the proposed PhC-NPQIC sensor device is potentially a promising platform for refractive index based biochemical sensing and lab-on-chip applications.

Acknowledgements

The authors thank Dr. Qimin Quan (Rowland Institute at Harvard) and Prof. Marko Lončar (Harvard university) for valuable discussions. This research was supported by NSFC (No. 61372038), National 973 Program (No. 2012CB315705), National 863 Program (No. 2011AA010306) and Fund of State Key Laboratory of Information Photonics and Optical Communications (BUPT), PR China.

References

[1] R. Daw, J. Finkelstein, Lab on a chip, Nature 442 (7101) (2006) 367–418.
[2] X. Fan, I.M. White, S.I. Shopova, H. Zhu, J.D. Suter, Y. Sun, Sensitive optical biosensors for unlabeled targets: a review, Anal. Chim. Acta 620 (1–2) (2008) 8–26.
[3] H.K. Hunt, A.M. Armani, Label-free biological and chemical sensors, Nanoscale 2 (2010) 1544–1559.
[4] J. Topolancik, P. Bhattacharya, J. Sabarinathan, P.-C. Yu, Fluid detection with photonic crystal-based multichannel waveguides, Appl. Phys. Lett. 82 (2003) 1143–1145.
[5] M. Loncar, A. Scherer, Y. Qiu, Photonic crystal cavity laser sources for chemical detection, Appl. Phys. Lett. 82 (2003) 4648–4651.
[6] E. Chow, A. Grot, I.W. Mirkarimi, M. Sigalas, G. Girolami, Ultracompact biochemical sensor built with two-dimensional photonic crystal microcavity, Opt. Lett. 29 (2004) 1093–1095.
[7] T. Xu, N. Zhu, M.Y.-C. Xu, Lech Wosinski, J. Stewart Aitchison, H.E. Ruda, Pillar-array based optical sensor, Opt. Express 18 (2010) 5420–5425.
[8] K. Yao, Y. Shi, High-Q width modulated photonic crystal stack mode-gap cavity and its application to refractive index sensing, Opt. Express 20 (2012) 27039–27044.
[9] C. Kang, C.T. Phare, Y.A. Vlasov, S. Assefa, S.M. Weiss, Photonic crystal slab sensor with enhanced surface area, Opt. Express 18 (2010) 27930–27937.
[10] D. Yang, H. Tian, Y. Ji, Nanoscale photonic crystal sensor arrays on monolithic substrates using side-coupled resonant cavity arrays, Opt. Express 19 (2011) 20023–20034.
[11] W. Lai, S. Chakravarty, Y. Zou, R.T. Chen, Silicon nanomembrane based photonic crystal microcavities for high sensitivity bio-sensing, Opt. Lett. 37 (2012) 1208–1210.
[12] W. Lai, S. Chakravarty, Y. Zou, Y. Guo, R.T. Chen, Slow light enhanced sensitivity of resonance modes in photonic crystal biosensors, Appl. Phys. Lett. 102 (2013) 041111.
[13] Q. Quan, F. Vollmer, I.B. Burgess, P.B. Deotare, I.W. Frank, S.K.Y. Tang, R. Illic, M. Loncar, Ultrasensitive on-chip photonic crystal nanobeam sensor using optical bistability, in: Quantum Electronics and Laser Science Conference (QELS), May 1, Baltimore, MD, 2011.
[14] D. Yang, H. Tian, Y. Ji, Q. Quan, Design of simultaneous high-Q and high-sensitivity photonic crystal refractive index sensors, J. Opt. Soc. Am. B 30 (8) (2013) 2027–2031.
[15] J. Jagerska, H. Zhang, Z. Diao, N. Le Thomas, R. Houdre, Refractive index sensing with an air-slot photonic crystal nanocavity, Opt. Lett. 35 (2010) 2523–2525.
[16] M.G. Scullion, A. Di Falco, T.F. Krauss, Slotted photonic crystal cavities with integrated microfluidics for biosensing applications, Biosens. Bioelectron. 27 (2011) 101–105.
[17] A. Di Falco, L. O'Faolain, T.F. Krauss, Chemical sensing in slotted photonic crystal heterostructure cavities, Appl. Phys. Lett. 94 (2009) 063503.
[18] B. Wang, M.A. Dundar, R. Ntzel, F. Karouta, S. He, R.W. Heijden, Photonic crystal slot nanobeam slow light waveguides for refractive index sensing, Appl. Phys. Lett. 97 (2010) 151105.
[19] R. Karlsson, SPR for molecular interaction analysis: a review of emerging application areas, J. Mol. Recogn. 17 (2004) 151–161.
[20] J.N. Anker, W.P. Hall, O. Lyandres, N.C. Shah, J. Zhao, R.P. Duyne, Biosensing with plasmonic nanosensors, Nat. Mater. 7 (2008) 442–453.
[21] C. Caucheteur, Y. Shevchenko, L. Shao, M. Wuilpart, J. Albert, High resolution interrogation of tilted fiber grating SPR sensors from polarization properties measurement, Opt. Express 19 (2011) 1656–1664.
[22] A. Ymeti, J.S. Kanger, J. Greve, G.A. Besselink, P.V. Lambeck, R. Wijn, R.G. Heideman, Integration of microfluidics with a four-channel integrated optical Young interferometer immunosensor, Biosens. Bioelectron. 20 (2005) 1417–1421.
[23] A. Ymeti, J. Greve, P.V. Lambeck, T. Wink, S. van Hovell, T.A.M. Beumer, R.R. Wijn, R.G. Heideman, V. Subramaniam, J.S. Kanger, Fast ultrasensitive virus detection using a young interferometer sensor, Nano Lett. 7 (2007) 394–397.

[24] J. Yang, L. Jiang, S. Wang, B. Li, M. Wang, H. Xiao, Y. Lu, H. Tsai, High sensitivity of taper-based Mach-Zehnder interferometer embedded in a thinned optical fiber for refractive index sensing, Appl. Opt. 50 (2011) 5503–5507.

[25] Y. Sun, X. Fan, Optical ring resonators for biochemical and chemical sensing, Anal. Bioanal. Chem. 399 (2011) 205–211.

[26] J.T. Robinson, L. Chen, M. Lipson, On-chip gas detection in silicon optical microcavities, Opt. Express 16 (6) (2008) 4296–4301.

[27] L.J. Sherry, S. Chang, G.C. Schatz, R.P. Van Duyne, Nano Lett. 5 (2005) 2034–2038.

[28] Q. Quan, P.B. Deotare, M. Loncar, Appl. Phys. Lett. 96 (20) (2010) 203102.

[29] A.M. Armani, K.J. Vahala, Opt. Lett. 31 (2006) 1896–1898.